Journal of The Electrochemical Society, **148** (5) A402-A410 (2001)
0013-4651/2001/148(5)/A402/9/$7.00 © The Electrochemical Society, Inc.

Electrochemistry of InSb as a Li Insertion Host

Problems and Prospects

K. C. Hewitt,* L. Y. Beaulieu,* and J. R. Dahn,z**

Department of Physics, Dalhousie University, Halifax, Nova Scotia, Canada B3H 3J5

Ballmilling of In and Sb has been used to produce InSb for use in electrochemical and *in situ* X-ray diffraction studies (XRD) of Li/1 M $LiPF_6$ ethylene carbonate:diethyl carbonate/InSb cells. The cell capacity decays rapidly when cycled between 0 and 1.3 V, while the capacity reduction is less pronounced when cycling is restricted to the 0.65-1.4 V range. *In situ* XRD studies reveal that Li_3Sb and In are formed during the first plateau (above 0.65 V), according to the reaction $3Li + InSb \rightarrow Li_3Sb + In$. The indium product subsequently reacts with Li forming the $InLi_x$ phases InLi and In_4Li_7 in sequence. When cells are cycled above 0.6 V (*i.e.*, in the absence of $InLi_x$ formation) capacity retention improves significantly, remaining relatively constant near 250 mAh/g. Detailed *in situ* XRD studies of these cells suggest that 0.27 Li atoms per InSb may be intercalated during a sharp drop in the cell potential, according to the reaction $xLi + InSb \rightleftharpoons Li_xInSb$ ($x_{max} = 0.27$). This intercalation accounts for only a small (about 30 mAh/g) fraction of the overall capacity of 680 mAh/g. Consequently, it appears that the reactivity of In and Sb with Li, not the structure type, determines the reaction path. Therefore, InSb is not an attractive intercalation host for Li, in contrast to the claims made in the literature.
 [DOI: 10.1149/1.1359194]

Manuscript submitted June 27, 2000; revised manuscript received December 28, 2000.

In the search for negative electrode (anode) materials for use in lithium-based batteries, it has been recently proposed[1] that intermetallic compounds with the zinc blende structure may be attractive candidates. The suggestion is derived in part from the availability of interstitial Li insertion sites as readily seen along a [110] projection of the zinc blende structure. At room temperature and atmospheric pressure InSb crystallizes in the cubic zinc blende structure ($F\bar{4}3m$ no. 216), and so in a recent paper[1] the electrochemical and structural characteristics of this prototype compound were tested to determine its effectiveness as a Li insertion host. It was reported that two Li atoms could be incorporated into InSb to form a hitherto unknown Li_2InSb phase that displays very little (5.6%), volume expansion (relative to InSb). The new phase was claimed to form according to the reaction $2Li + InSb \rightarrow Li_2InSb$, while a subsequent reaction $xLi + Li_2InSb \rightarrow Li_{2+x}In_{1-x}Sb + xIn$ ($x_{max} = 1$) forms Li_3Sb and In. The electrochemical cell exhibited good capacity retention (300 mAh/g) over 22 cycles. This prompted the authors to suggest that the results open up exciting possibilities for identifying other zinc blende insertion electrodes.

Earlier work (not referenced by the authors of Ref. 1) on the reaction of lithium with InSb showed that only a small amount of Li could be intercalated within the InSb structure from solutions of *n*-butyllithium in hexane. Herren and Walsoe de Reca[2] found $x = 0.053$ in Li_xInSb was the limiting composition under these conditions.

As suggested by the authors of Ref. 1, further work is required to determine the exact structural transformations that occur during the discharge and charge of InSb electrodes. For example, InSb and Li_3Sb have very similar *a* axis lattice parameters and structure (cubic). Consequently, one may mistakenly identify one phase for the other except for the presence of a [200] reflection that is present in the X-ray diffraction (XRD) pattern of Li_3Sb and not InSb. This difference is, in part, based on the fact that In and Sb have similar atomic scattering factors while Li and Sb do not. In addition, the appearance of In along with Li_3Sb in the diffraction pattern is another important determinant of the reaction process. It is with these considerations in mind that we conducted *in situ* XRD and electrochemical studies of Li/InSb cells. To better understand the reaction of Li with InSb, the electrochemistry of cycled Li/Sb cells and the associated structural changes in the Sb electrode were also studied.

The electrochemical studies reveal that Li/InSb cells exhibit a rapid drop in capacity with cycle number when cycled (50 times) between 0 and 1.3 V. Conversely, cell capacity is retained at approximately 250 mAh/g over the first 12 cycles when the voltage lies in the range 0.65-1.4 V, in agreement with the results found in Ref. 1. *In situ* XRD studies of cells cycled between 0 and 1.3 V reveal that In and Li_3Sb are formed during the first discharge plateau (above 0.65 V), while $InLi_x$ ($x = 1$ and $x = 1.75$) phases are formed at lower voltages during the first discharge. More detailed *in situ* XRD studies of cells cycled between 0.6 and 1.4 V suggest that a small fraction (0.27 per InSb) of Li can be reversibly intercalated. Insertion occurs during the initial moments of discharge while extraction presumably occurs during the final moments of charging, in accord with the reaction $xLi + InSb \rightleftharpoons Li_xInSb$ ($x_{max} = 0.27$). A dramatic decrease in the cell potential characterizes the period of intercalation while the period of deintercalation is characterized by a dramatic increase in the cell potential. At the end of the intercalation period, Li_3Sb and In are formed during the subsequent plateau (above 0.65 V) with a concomitant reduction in InSb content, in accordance with the reaction $(3 - x_{max})Li + Li_{x_{max}}InSb \rightarrow In + Li_3Sb$.

Experimental

InSb synthesis.—In an argon glove box ($[H_2O]$, $[O_2] < 1$ ppm), indium shot (Cominco Electronics, 69 grade) and antimony powder were mixed in a 1:1 mole ratio (total mass approximately 2 g). Within the same glove box, along with two or four hardened stainless steel balls (1/2 in. diam, mass = 8.2 g), the mixture was sealed in a hardened stainless steel ballmilling container (BMC). The reactants were ballmilled at room temperature for 20 h using a Spex 8000 mixer mill. After opening the BMCs in an argon glove box, a small quantity of the recovered black powder was placed in an X-ray holder. The holders' base is made of Si(510), which does not contribute to scattering because the structure factor of the (510) reciprocal lattice plane of silicon is zero. The cover of the holder is composed of thin aluminized Mylar formed in a circular arc that is perpendicular to, and outside the focal plane of, the incident X-ray beam. Combined with an O-ring system, this holder[3] serves to isolate the powder from air, and although it attenuates the incident and scattered X-ray beam, it does not add peaks to the pattern.

XRD experiments were carried out using a Siemens D5000, Siemens D500, or Philips PW1720 diffractometer equipped with a Cu target X-ray tube and a diffracted beam monochromator (selecting Kα radiation). The systems are arranged in the Bragg-Brentano

* Electrochemical Society Student Member.
** Electrochemical Society Active Member.
z E-mail: jeffdahn@is.dal.ca

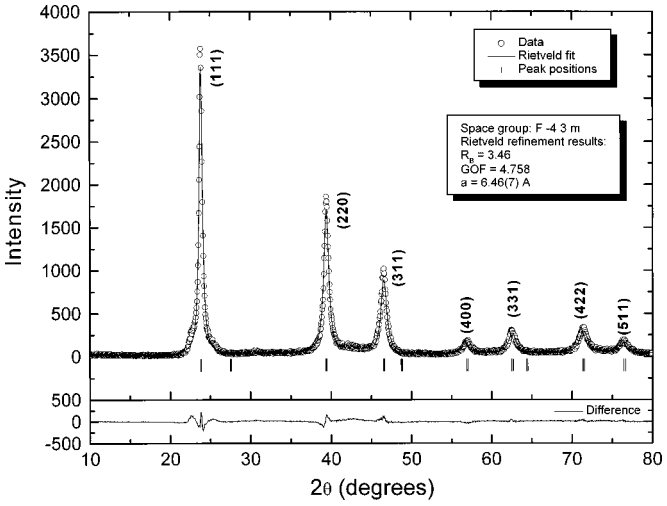

Figure 1. XRD pattern (points) of InSb and a theoretical pattern (solid line) derived from a Rietveld refinement using the space group $F\bar{4}3m$ (no. 216). The difference (lower panel) between theory and experiment is small, indicating that cubic zinc blende InSb has been synthesized.

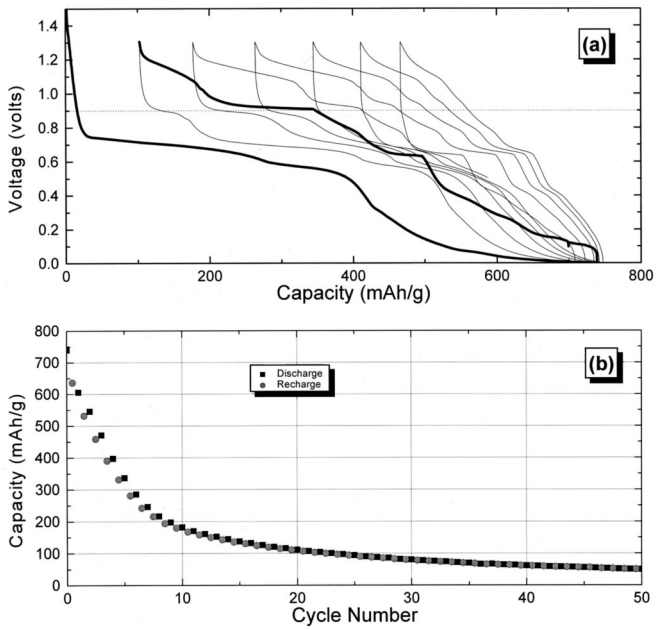

Figure 2. (a) Voltage *vs.* specific capacity and (b) specific capacity *vs.* cycle number of a Li/1 M $LiPF_6$ EC:DEC/InSb cell cycled between 0 and 1.3 V. The first discharge-charge cycle is given by the bold line.

(flat-plate sample) geometry. Fixed divergence slits are used with each of these instruments.

The XRD pattern of the black powder recovered from ballmilling In and Sb (Fig. 1) is found to persist even upon air exposure for 1 day. Using four balls instead of two in the ballmilling procedure results in an increase in impurity (<1% Fe) concentration so powder from the two-ball synthesis process was used for analysis and cell preparation. A Rietveld refinement of the XRD pattern was carried out using *Powder Cell for Windows (Version 2.3)*. The refinement (see Fig. 1) was completed using the space group $F\bar{4}3m$ (no. 216), resulting in an *a* axis lattice parameter of magnitude 6.46(7) Å. Therefore, ballmilling In and Sb at room temperature and atmospheric pressure has successfully produced InSb with the cubic zinc blende structure

Electrochemical Cell Construction

A slurry is produced by combining a sample (~300 mg) of InSb (45 μm mesh) with 8 wt % Super S carbon black (MMM Carbon, Belgium), 100 wt % of 10% Kynar 301F polyvinylidene fluoride (PVDF, Elf-Atochem) in *N*-methyl-2-pyrrolidinone (NMP) and approximately 120 wt % NMP. This combination is then mixed in a small cuvette with four (3.15 mm diam, 0.1 g) small stainless steel balls and shaken for 1-2 h using a Thermolyne (model M37600) Maxi Mix II. The resulting slurry is drawn into a thin (275 μm) layer on 10 μm copper foil using a 0.011 in. notch bar (homemade). For Sb-based samples a 0.003 in. notch bar is used, resulting in a 100 μm thick coating on Cu foil. NMP is subsequently lost upon drying the coated copper foil for 1.5 h in air at 75-80°C, leaving 85 wt % InSb (or Sb), 7 wt % carbon black, and 8 wt % by PVDF.

Standard 2325 size coin cells are produced in the following manner. First, 13 mm diam disks are punched-out from the coated copper foil, the slurry mass (approximately 10 mg) being determined by subtracting the mass of a similarly punched but uncoated region of the same copper foil. The electrode and cell parts are transferred to an argon glove box where the InSb electrode is placed in a standard battery cell can. A few drops of the electrolyte 1 M $LiPF_6$ ethylene carbonate (EC):diethyl carbonate (DEC) (33:67 volume ratio) (Mitsubishi Chemical) are added. The InSb electrode is then separated from Li metal foil (FMC Corporation) by a Celgard no. 2502 polypropylene microporous separator. A stainless steel spacer (18 mm diam, ~1 mm thick), disk spring (17 mm diam), and cover complete the electrochemical sandwich.

For *in situ* experiments a similar sample preparation and construction scheme is used except that the slurry is applied directly to a Be disk, which is transparent to X-rays. Or, alternatively, a Be window is placed opposite the coated copper. The beryllium window covers the opening of a can and is attached to it after the application of three coats of Roscobond pressure sensitive adhesive. Construction of the cell is completed as describe before and is protected from possible electrolyte leakage by applying Torr Seal (Varian) at the Be window-can joint. In the first case (coated Be windows) X-rays pass directly through the Be window onto InSb, while in the second case X-rays pass through (in sequence) the Be window, Li foil, separator, and electrolyte before impinging upon the InSb electrode. Both methods have been used, the latter one being employed to facilitate direct comparison with cells produced by the coated copper foil method. On the other hand, in the coated Be window method the X-rays pass through one instead of multiple layers providing a better signal/noise ratio. In addition, the mass of laminated Be window electrodes are typically three times that of the laminated copper foil electrodes. As such, *in situ* XRD experiments of coated Be windows are more sensitive to changes in the phases present during cycling. Both types of *in situ* experiments are presented here.

InSb electrode function.—Cells were tested using constant charge and discharge currents (150-180 μA) at a temperature of 30.0 ± 0.1°C. The theoretical gravimetric capacity of a Li/InSb cell is 679 mAh/g for Li_3Sb and $InLi_3$ formation and 793 mAh/g if Li_3Sb and $InLi_4$ are formed at the end of the discharge. As can be seen in Fig. 2a, the Li/InSb cell achieves about 740 mAh/g during the first discharge to 0 V. This observation is consistent with the formation of Li_3Sb and $InLi_x$ phases. There is, however, a dramatic drop in capacity with increasing cycle number (Fig. 2b). Correlated with this reduction is the shortening of the second charge plateau seen in Fig. 2a at 0.9 V, as well as other changes to the voltage profile. The experiment was completed on three separate cells prepared in the same manner, resulting in identical results for each.

In situ X-ray diffraction: part 1, 0.0-1.3 V.—In order to identify the phases formed during cycling between 0 and 1.3 V, *in situ* XRD of cells prepared with InSb coated on Be windows were studied

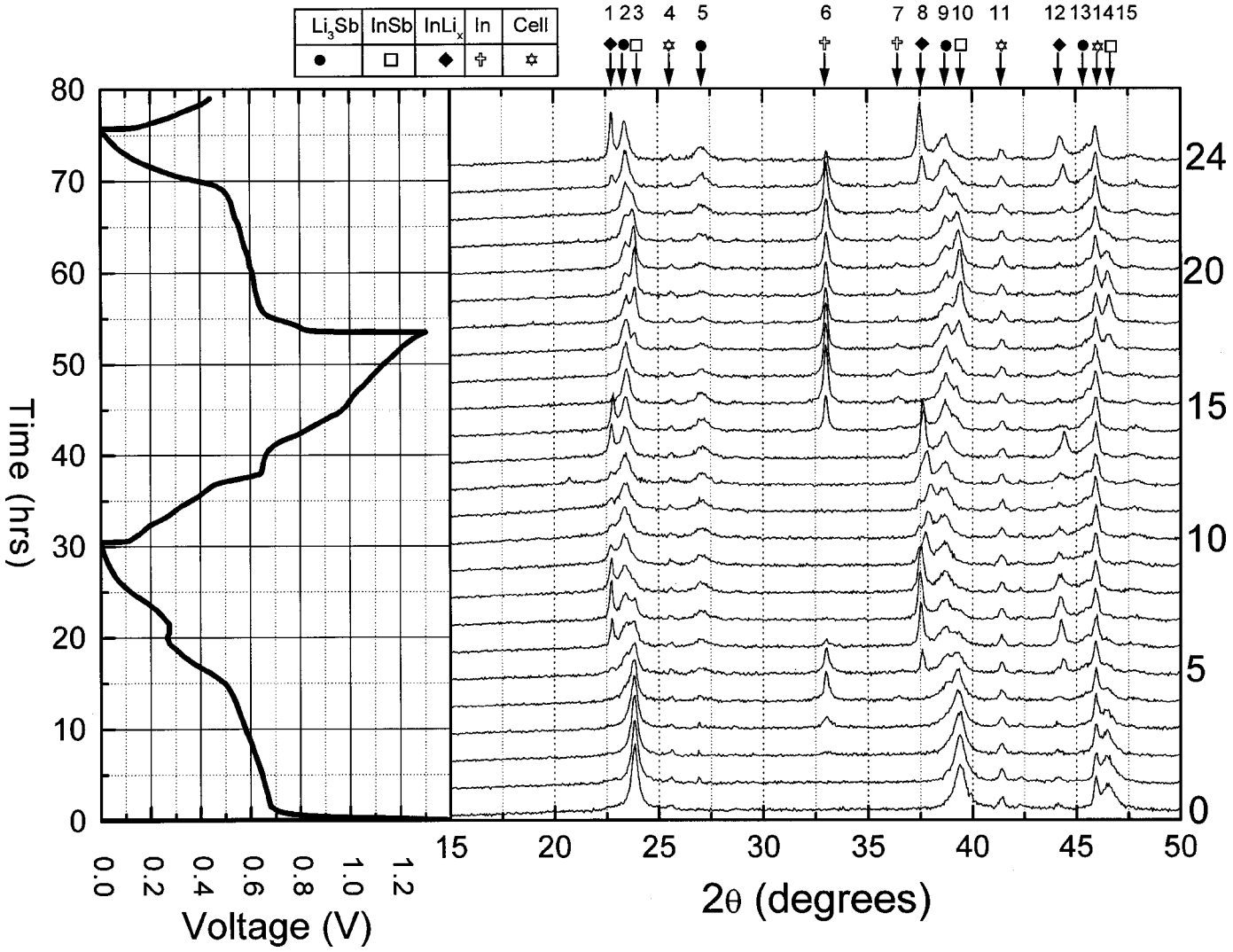

Figure 3. *In situ* XRD patterns of the InSb electrode of a Li/InSb cell cycled between 0 and 1.3 V.

during a C/30 charge-discharge cycle (400 μA discharge/charge current). *In situ* XRD patterns, each of 3 h duration, were collected during the first discharge, first charge, and second discharge cycles. The first of these XRD patterns is a scan of the fresh cell before discharge begins. These patterns and the associated time-synchronized voltage curve are shown in Fig. 3.

The peaks in the XRD patterns have been identified as described in Table I. InSb, Li_3Sb, and In peaks were indexed from the XRD pattern at the top of charge (scan 18), InLi peaks were indexed from scan 7, and $InLi_{1.75}$ peaks were indexed from scan 11, resulting in the lattice parameters listed in Table II. Also given in Table II are the literature values of the lattice constants from the JCPDS file.

The InSb electrode phase composition evolves qualitatively in the following manner. During the first plateau (scans 1-5) it can be seen (Fig. 3) that indium (peak 6) and Li_3Sb (peak 9 most notably) peaks grow at the expense of InSb. For the latter half (6-10) of the discharge cycle, as indium metal peaks are reduced in intensity InLi phase peaks (no. 1, 8, 12) appear with continued growth of the Li_3Sb phase. By the bottom of the first discharge cycle InSb has disappeared completely (peaks 3, 10, 14 are absent), being replaced by Li_3Sb and $InLi_{1.75}$ phases.

The first two scans (11 and 12) during charge show little change, except for the production of different $InLi_x$ phases as deduced from the changing 2θ values of peaks 1, 8, and 12. $InLi_x$ related peaks

Table I. Nominal scattering angle, 2θ, Miller [*hkl*] index and phase identification for peaks seen in the *in situ* XRD patterns of an InSb electrode cycled against Li between 0 and 1.3 V.

Peak	2θ	[*hkl*]	Phase[a]
1	22.7-22.8	(111)	$InLi_x$
2	23.6	(111)	Li_3Sb
3	23.9	(111)	InSb
4	25.6		Cell hardware
5	27.3	(200)	Li_3Sb
6	33	[101]	In
7	36.5	(002)	In
8	37.5-36.0	(220)	$InLi_x$
9	38.9	(220)	Li_3Sb
10	39.45	(220)	InSb
11	41.4		Cell hardware
12	44.2-44.3	(311)	$InLi_x$
13	45.5	(311)	Li_3Sb
14	45.9	(100)	Beryllium
15	46.6	(311)	InSb

[a] $1 \leqslant x \leqslant 1.75$ for $InLi_x$.

Table II. Crystal structure parameters for each phase observed in the charge/discharge of an InSb electrode cycled against Li between 0 and 1.3 V.

Phase	No. peaks indexed	Space group	System	Lattice parameter(s)	Literature values (Å)	JCPDS no.
InSb	3	$F\bar{4}3m$ (no. 216)	Cubic	a = (6.466 ± 0.003) Å	a = 6.4782	6-208
Li_3Sb	4	$Fm\bar{3}m$ (no. 225)	Cubic	a = (6.562 ± 0.006) Å	a = 6.572	4-791
InLi	3	$Fd\bar{3}m$ (no. 227)	Cubic	a = (6.785 ± 0.003) Å	a = 6.786	3-908
In_4Li_7	3	$Fd\bar{3}m$ (no. 227)	Cubic	a = (6.72 ± 0.03) Å	a = 6.733	Ref. 4
In	2	$I4/mmm$ (no. 139)	Tetragonal	a = 3.24(7) Å c = 4.93(0) Å	a = 3.2517 c = 4.9459	5-642

appear at two distinct sets of scattering angle (see scans 8-12, near 38°). Thus one may deduce that two $InLi_x$ phases are present during cycling. An examination of the phase diagram[4] of In-Li shows a series of phases for increasing Li content: In, InLi, In_4Li_7, $InLi_2$,

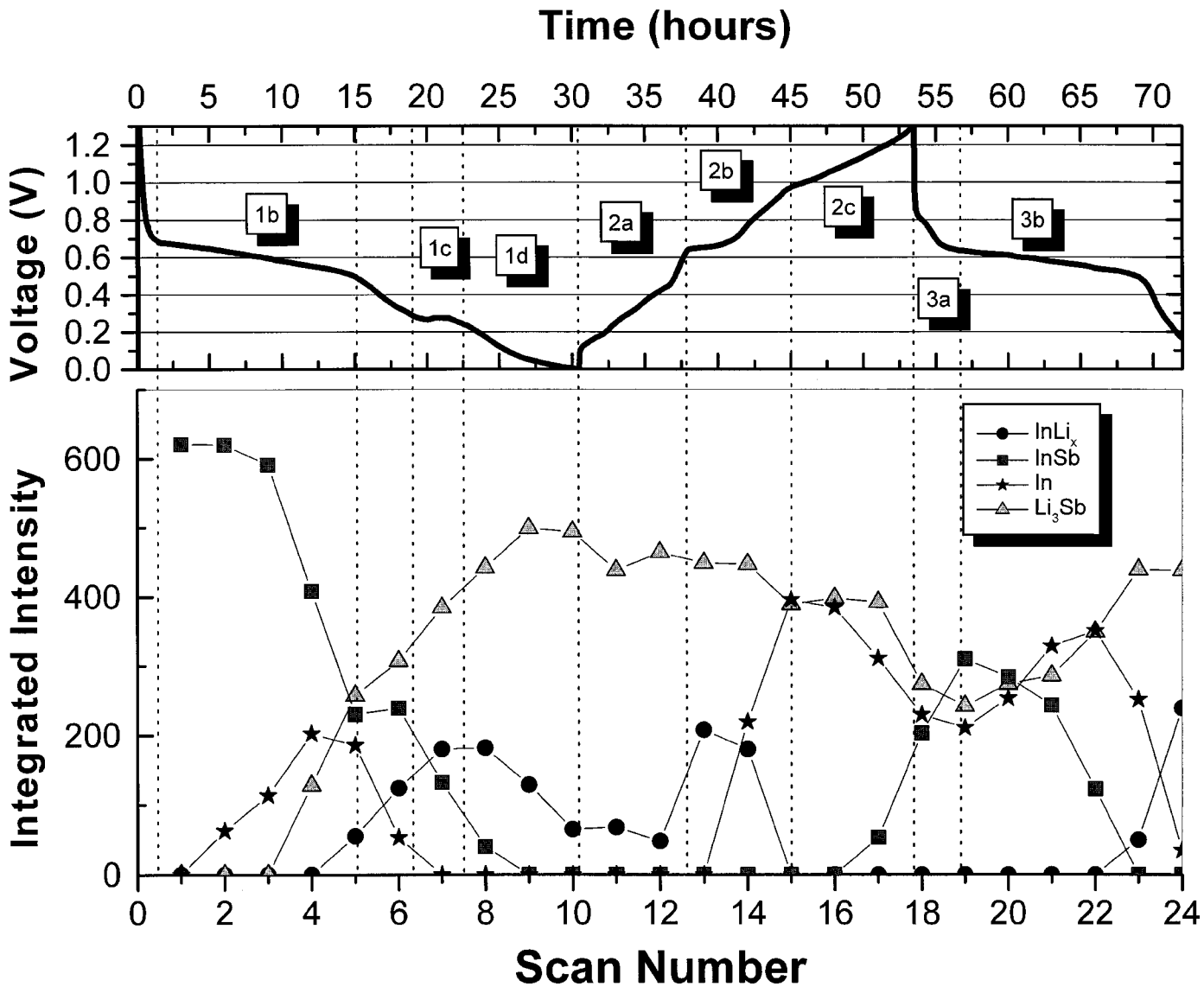

Figure 4. Integrated intensity of the In(101), InSb(111), Li_3Sb(111), and $InLi_x$(111) peaks as a function of scan number, during the first 1.5 cycles of a Li/InSb cell discharged to a potential of 0 V.

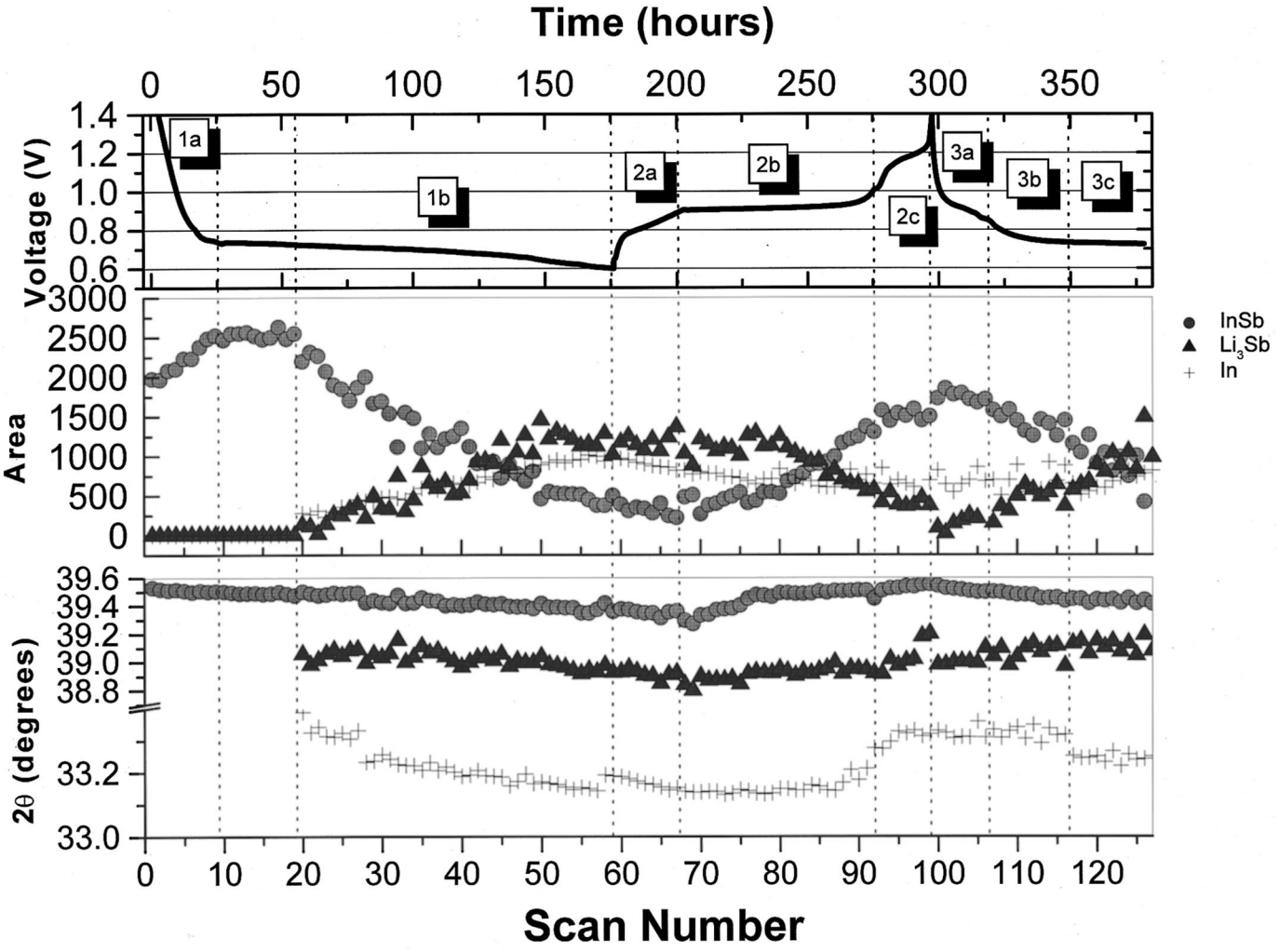

Figure 5. Integrated intensity of In(101), InSb(220), and Li_3Sb(220) peaks as a function of scan number, during the first 1.5 cycles of a Li/InSb cell above 0.6 V.

In_3Li_8, $InLi_3$, $InLi_4$ (*i.e.*, $InLi_x$, $0 \leq x \leq 4$, for T = 25-50°C). In the phase diagram, In and InLi phases coexist for Li content between 1.5 and 46.5 atom %. Consequently, one may deduce that peaks 1, 8, and 12 in scan 5 are due to InLi since one also observes indium peaks (6, 7) as well. The next pair of phases (InLi and In_4Li_7) also coexist at room temperature and explain the peaks observed in scans 10 and 11. These arguments suggest that during cycling InLi and $InLi_{1.75}$ phases form. InLi crystallizes in the face-centered cubic (fcc) NaTl-type structure (space group $Fd\bar{3}m$, no. 227) with a cubic lattice parameter a = 6.786 Å.[4] XRD patterns 10 and 11 indicate that the In_4Li_7 phase must have a cubic structure with a shortened a axis parameter. Indeed, this phase is found[4] to have a cubic lattice parameter of 6.733 Å, consistent with the results presented here (see Table II).

During the first charge plateau one observes significant changes in the XRD pattern. In particular, the InLi phase peaks of scans 13 and 14 now lie at the same scattering angles seen in scan 5 and disappear completely by scan 15. So, while $InLi_x$ phases seem to be removed completely upon cycling this is not true of Li_3Sb, which remains at the top of charge (scan 18). Li_3Sb peaks are always observed in all scans after no. 2 and 3. So, while $InLi_x$ cycles well a portion of Li_3Sb is retained at the anode. The latter observation may explain the poor cycling behavior of these cells.

In order to quantify the changes in the proportion of each phase, all peaks of the various phases are fit to Lorentzian line-shape profiles with overlapping peaks being fit using combined multiple peak fits. For any particular phase, the changes in integrated intensity and scattering angle are found to be independent of the peak chosen. Therefore, in the following discussion only the results from one selected peak of each phase are presented (Fig. 4).

During the first discharge cycle, the growth in intensity of the [111] Li_3Sb and [101] In reflections show that these phases are formed with a reduction in the InSb phase during the first discharge plateau (1b). The Li_3Sb peaks index well to a BiF_3-type cubic structure with space group $Fm\bar{3}m$ (no. 225; a = 6.562 ± 0.006 Å) while the In peaks index well to a tetragonal $I4/mmm$ [no. 139; a = 3.24(7) Å, c = 4.92(9) Å] structure. There is no evidence of the formation of a Li_2InSb phase at any potential as reported in Ref. 1.

$InLi_x$ phases are formed below 0.5 V (see scan 5) and InSb, as measured by the intensity of the [111] reflection, disappears at the end of the first discharge (1d). Thus it would appear that the reaction sequence is as follows: 3 Li + InSb → Li_3Sb + In (1b); In + Li → InLi (1c); and InLi + 0.75 Li → $InLi_{1.75}$ (1d). Since Li_3Sb remains after the initial moments of the first cycle, it would seem that Reaction 1b is limited in its reversibility, while $InLi_x$ cycles well (*i.e.*, reaction 1c is reversible).

In situ X-ray diffraction: part 2, coated Cu foil.—The experiments that showed good cycling performance in Ref. 1 were re-

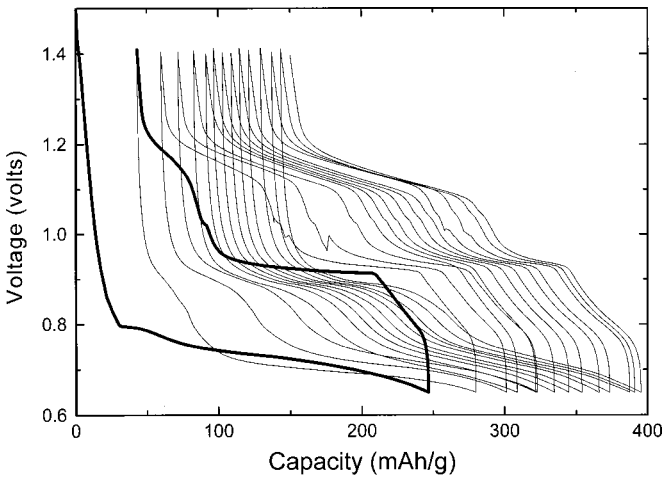

Figure 6. Voltage *vs.* specific capacity for a Li/InSb cell cycled between 0.65 and 1.4 V. The first discharge-charge cycle is given by the bold line.

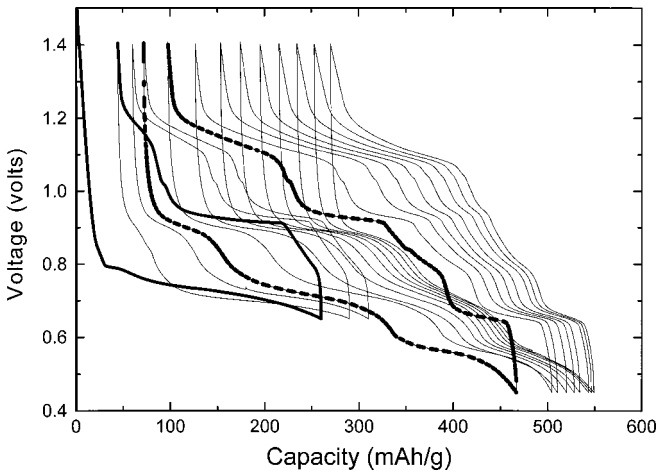

Figure 8. Voltage *vs.* specific capacity for a Li/InSb cell cycled between 0.45 and 1.4 V. The first discharge-charge cycle is given by the bold line and the first discharge charge cycle to 0.45 V is given by the bold dashed line.

stricted to potentials above 0.5 V, where it was claimed that Li_2InSb formed. The experiments reported in Fig. 3 and 4 did not detect such a phase, but they were made at relatively high rates of discharge. In order to be sure of the initial reaction path, we performed a second *in situ* XRD experiment at about C/300 where the potential was changed in the range $0.6\,V < V < 1.4\,V$.

This *in situ* XRD study of the cycling behavior of Li/InSb cells between 0.6 and 1.4 V was conducted using the coated Cu foil electrodes. These experiments are more detailed than the first in that a longer discharge time (*i.e.*, a 28 μA constant current applied to a 13 mg active mass) is used. Lorentzian fits were made to all observed peaks.

During the sharp drop in voltage (1a) on the first discharge (Fig. 5), the only observed change is a growth in the integrated intensity of InSb peaks (*e.g.*, [111] reflection), all others remaining constant within experimental noise. This change is possibly due to the intercalation of Li, since the introduction of an additional scattering center (Li) will increase the scattered intensity. How much Li could be intercalated? The sharp reduction in voltage (to about 0.72 V) accounts for about 30 mAh/g of the overall capacity of 679 mAh/g. This means that about 0.27 atoms of Li are inserted per InSb to form a $Li_{0.27}InSb$ phase, according to the reaction xLi + InSb → Li_xInSb ($x_{max} = 0.27$). In Ref. 2 a composition of $x = 0.053$ was obtained for InSb exposed to *n*-butyllithium in hexane which is known to correspond to a potential of about 1 V *vs.* Li. This is consistent with our results.

Further reaction of Li results in the production of In (*e.g.*, [101] reflection increase) and Li_3Sb ([111] reflection intensity increase) during the first plateau (1b in Fig. 5), according to Reaction 1b. In the process InSb is used up, resulting in a consequent reduction in the intensity of InSb peaks. During the portion of the charge labeled 2a in Fig. 5, no observable changes in the phases are observed. This may imply some range of lithium composition for the Li_3Sb phase. During 2b the InSb content increases while the Li_3Sb and In contents are reduced. Thus, Reaction 1b seems to be completely reversible. Combined with the conclusions of experiment 1, it would seem that Reaction 1c or 1d somehow limits the reversibility of Reaction 1b.

It is now time to critically compare our results to those in Ref. 1. Figure 2 in Ref. 1 shows diffraction patterns of fresh, dischaged (0.5 V) and charged electrodes. The diffraction pattern of the discharged electrode was assigned to the hypothetical Li_2InSb phase plus peaks assigned to the quartz diffraction holder and a stainless steel current

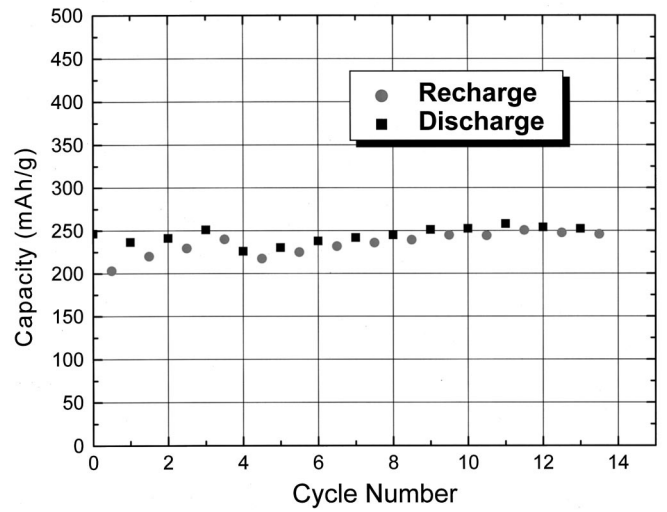

Figure 7. Specific capacity *vs.* cycle number for a Li/InSb cell cycled between 0.65 and 1.4 V.

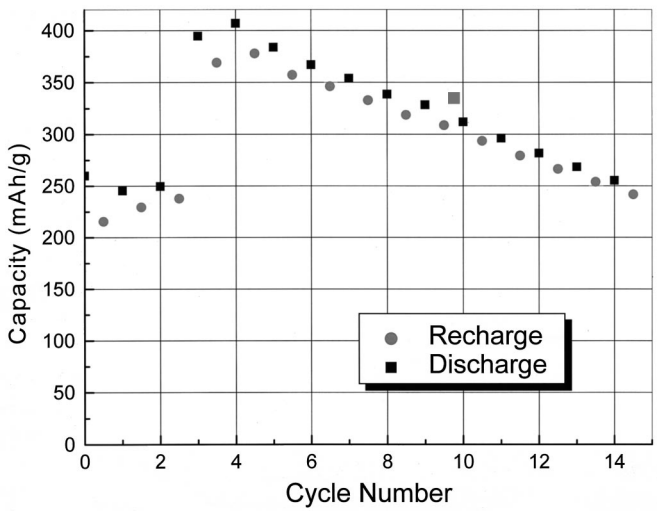

Figure 9. Specific capacity *vs.* cycle number for a Li/InSb cell cycled between 0.45 and 1.4 V.

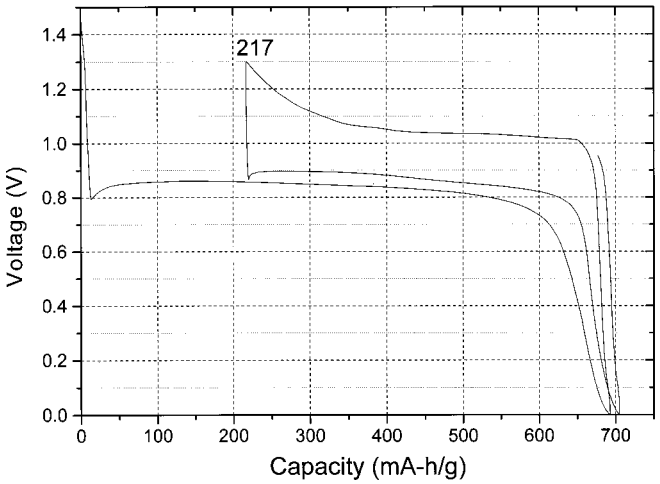

Figure 10. Voltage *vs.* specific capacity for a Li/Sb cell cycled between 0-1.3 V.

collector. However, a close examination of that pattern clearly shows that the peak at about 27°, assigned to stainless steel, is the [200] reflection from Li_3Sb, and the peak at 33°, assigned to the quartz holder, is the [101] reflection from indium. The peaks assigned to the Li_2InSb phase are those of Li_3Sb. Actually, the pattern for the discharged electrode in Ref. 1 agrees well with our patterns at about the same potential (for example, scan 5 in Fig. 3 and scan 60 in Fig. 5). We can only conclude that the authors of Ref. 1 made a spurious assignment of the peaks in their diffraction pattern, leading to an incorrect hypothesis about the existence of a Li_2InSb phase. In fact, in a recent conference presentation,[5] the authors of Ref. 1 admit this to be the case and report that In extrusion from InSb occurs at fairly small levels of lithiation, in agreement with our results.

The authors of Ref. 1 employed an annealing step in preparing their samples of InSb. The present work does not include this procedure which involves heat-treatment at 400°C for 12 h under flowing argon. This annealing treatment may have the effect of increasing the crystallite size. It is expected that increasing the size of the crystals would reduce the diffusion of Li and consequently kinetic effects may play a greater role. Thus, annealing at high temperature may lead to a decrease in the already minor amount of Li that can be reversibly inserted, *i.e.*, a reduction in x_{max} at a given charge/discharge rate.

In order to assess whether the reversibility of Reaction 1b is maintained over a number of cycles, a Li/InSb (12 mg active mass) cell was cycled between 0.65 and 1.4 V for two cycles at constant

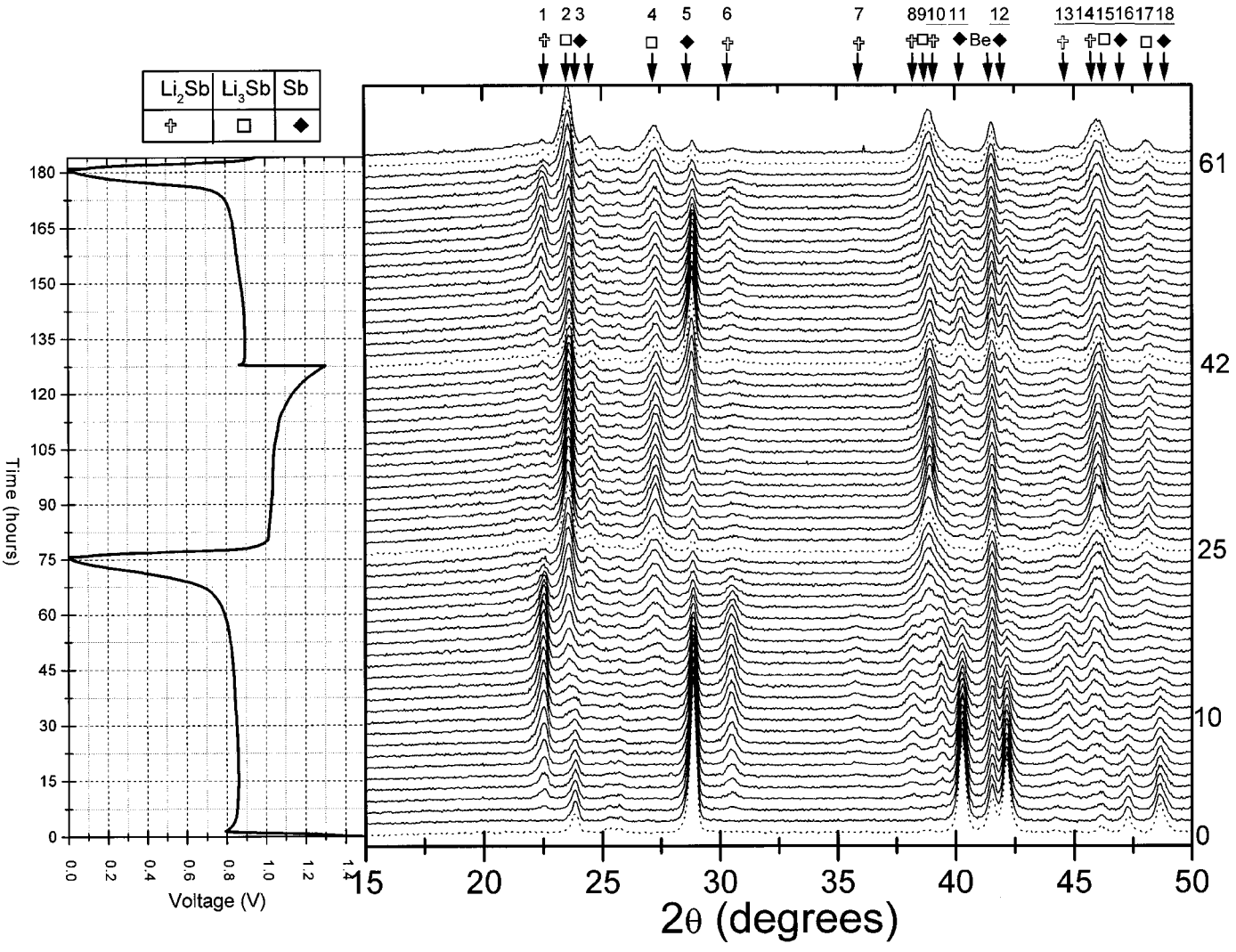

Figure 11. *In situ* XRD patterns of the Sb electrode of a Li/Sb cell.

Table III. Nominal scattering angle, 2θ, Miller [*hkl*] index, and phase identification for peaks seen in the *in situ* XRD patterns of an Sb electrode cycled against Li between 0 and 1.3 V.

Peak	2θ	[*hkl*]	Phase
1	22.5	(110)	Li_2Sb
2	23.6	(111)	Li_3Sb
3	23.8	(003)	Sb
4	27.3	(200)	Li_3Sb
5	28.9	(012)	Sb
6	30.5	(101)	Li_2Sb
7	35.8	(111)	Li_2Sb
8	38.2	(201)	Li_2Sb
9	38.9	(220)	Li_3Sb
10	39.4	(300)	Li_2Sb
11	40.3	(104)	Sb
12	42.1	(110)	Sb
13	44.8	(211)	Li_2Sb
14	45.8	(220)	Li_2Sb
15	46.0	(311)	Li_3Sb
16	47.3	(015)	Sb
17	48.1	(222)	Li_3Sb
18	48.7	(006)	Sb

charge/discharge current of 80 μA and then for ten cycles at double this current. Over these 12 cycles the gravimetric capacity is not significantly reduced in agreement with the results in Ref. 1 (see Fig. 6 and 7). The charge-discharge cycles shift to the right, indicating that Li remains incorporated in the InSb electrode (possibly because not all Li is removed from Li_3Sb upon charge). The voltage profile also changes shape dramatically during these first 12 cycles, for reasons that we have not yet investigated.

On the other hand, after cycling two times between 0.65 and 1.4 V, cycling ten times between 0.45 and 1.4 V does reduce the gravimetric capacity (see Fig. 8 and 9). As found earlier, by reducing the voltage below 0.6 V, the cycling performance is reduced. When the lower cutoff is reduced to 0.5 V, InLi is formed through Reaction 1c, and this seems to limit the reversibility of Reaction 1b, contributing to the observed capacity reduction.

Li/Sb electrode function.—In order to assess the nature of the reversibility of Reaction 1b further and to determine the identity of plateaus seen in Li/InSb cells, Li/Sb electrochemical cells were studied. The latter cell was cycled at a constant 207 μA charge/discharge current. The cell achieved a discharge capacity of 660 mAh/g, as expected for Li_3Sb formation, but loses about 217 mAh/g in capacity after the first cycle (Fig. 10).

Figure 11 shows the results of an *in situ* XRD study on a Li/Sb cell. The peaks of the phases that form sequentially are identified as listed in Table III. The peaks of each phase were indexed for scans 9 and 28 and refined to determine the lattice parameters listed in Table IV.

The electrochemical reactions that occur in a Li/Sb cell have been determined by other workers,[6] and are consistent with the reaction sequence deduced during the discharge cycle here, namely, $2Li + Sb \rightarrow Li_2Sb$ (a) and $Li + Li_2Sb \rightarrow Li_3Sb$ (b). Figure 11 shows that Reaction b begins to forms Li_3Sb by scan 10 (*i.e.*, approximately halfway) during the first discharge cycle, as is evident from the growth of the strongest Li_3Sb peak (no. 2) as a shoulder on the low angle side of the (003) Sb peak (no. 3). The behavior during charge is very different. No evidence of Li_2Sb is observed during any part of the charge cycle, and instead, Li_3Sb converts directly back to Sb as Li is removed. Li_3Sb peaks (2, 4, 9, 15, 17) are still present at the top of the first charge cycle, which should correspond to the complete removal of Li from the active material. Li_2Sb peaks (no. 1, 6, 7, 8, 10, 13, and 14) reappear during the second discharge. The hysteresis in the charge-discharge behavior of Li/Sb cells is not understood.

Table IV. Crystal structure parameters for each phase observed in the charge/discharge of a Sb electrode cycled against Li between 0 and 1.3 V.

Phase	No. peaks indexed	Space group	System	Lattice parameter(s) (Å)
Li_3Sb	5	$Fm\bar{3}m$ (no. 225)	Cubic	$a = (6.545 \pm 0.002)$
Li_2Sb	7	$P62c$ (no. 190)	Hexagonal	$a = (7.918 \pm 0.003)$ $c = (3.242 \pm 0.002)$
Sb	6	$R\bar{3}m$ (no. 166)	Hexagonal	$a = (4.288 \pm 0.003)$ $c = (11.226 \pm 0.006)$

Figure 12 compares the voltage profiles of Li/Sb and Li/InSb cells. Close examination of Fig. 12a, b, and c reveals that the first discharge cycle is different from subsequent ones. For Li/InSb cells a plateau develops on the second charge cycle around 0.9 V (Fig. 12a and c). After the third full cycle this plateau is shortened significantly. For Li/Sb cells a similar trend is observed, the development of two distinct plateaus (at 0.90 and 0.85 V) from the one gradually sloped plateau observed during the first discharge. This implies that the reactions forming Li_2Sb (0.90 V) and Li_3Sb (0.85 V) in Li/Sb cells are becoming distinguished from one another. The appearance of a 0.90 V plateau during Li/InSb cell discharge may suggest that Li_2Sb is being formed.

During charging there are also dramatic changes to the voltage profile with cycle number. For Li/InSb cells, the 0.9 V plateau present during charge is significantly shortened (Fig. 12a and c), and another plateau near 1.15 V grows in length as shown in Fig. 12c. The relative changes in these plateau lengths may be caused by formation of Li_2Sb during later cycles, but further experiments are needed to understand these effects.

Conclusions

It was found that electrochemical cycling of a Li/InSb cell results in the initial insertion of Li into interstitial sites in the cubic zinc blende InSb structure at the beginning of the discharge cycle. This insertion accounts for only about 30 mAh/g of the overall capacity and hence to an insertion of 0.27 Li atoms per InSb (*i.e.*, $Li_{0.27}InSb$). During the first plateau (above 0.65 V) in the discharge cycle, Li_3Sb and In are formed, and at the second plateau (around 0.5 V) $InLi_x$ ($1 \leq x \leq 1.75$) phases are formed. The $InLi_x$ phases convert back to In reversibly during charge, but some Li_3Sb is detected in

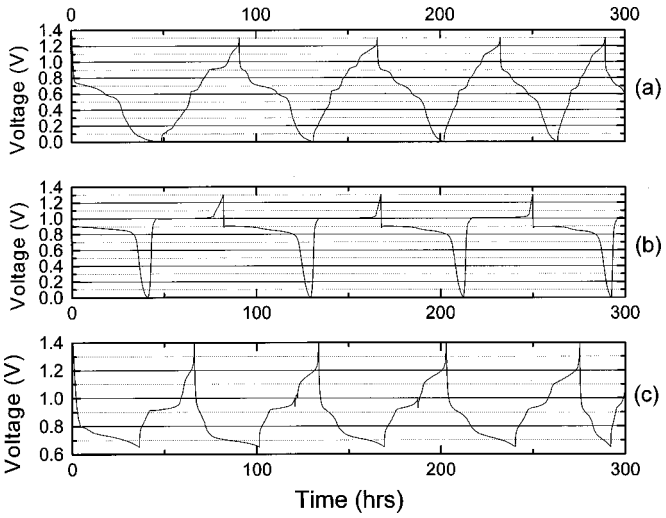

Figure 12. Voltage profiles of the first few cycles of (a) Li/InSb (0.0-1.4 V), (b) Li/Sb (0.0-1.3 V), and (c) Li/InSb (0.65-1.4 V) cells.

charged electrodes. The limited reversibility of the extraction of Li from Li_3Sb results in a decrease in cell capacity with cycling. In summary, the overall reaction sequence during discharge is as follows

$$x\mathrm{Li} + \mathrm{InSb} \rightarrow \mathrm{Li}_x\mathrm{InSb} \quad (x_{\max} = 0.27) \qquad [1a]$$

$$(3 - x)\mathrm{Li} + \mathrm{Li}_x\mathrm{InSb} \rightarrow \mathrm{Li}_3\mathrm{Sb} + \mathrm{In} \qquad [1b]$$

$$\mathrm{In} + \mathrm{Li} \rightarrow \mathrm{InLi} \qquad [1c]$$

$$\mathrm{InLi} + 0.75\,\mathrm{Li} \rightarrow \mathrm{InLi}_{1.75} \qquad [1d]$$

The reactions during the first charge are the reverse of those shown above. As Li/InSb cells cycle, there are profound changes to the voltage profile that may be caused by the formation of the thermodynamically stable Li_2Sb phase, which is not detected in the first cycle. To understand the changes in the voltage profile with cycle number would require a significant amount of work that would be hard to justify for a compound based on such exotic elements.

Since Li intercalation accounts for only about 5% of the overall capacity, it would appear that the reactivity of the elements rather than the structure is the most significant factor in determining the degree to which InSb can act as an intercalation host. Both In and Sb form alloys with Li and intercalation accounts for only a small fraction of the capacity. The case of other intermetallic compounds needs to be investigated, but our results imply that Li intercalation into intermetallic zinc blende structures has an extremely small capacity.

Acknowledgments

The support of NSERC, 3M Company, and 3M Canada Company is gratefully acknowledged.

Dalhousie University assisted in meeting the publication costs of this article.

References

1. J. T. Vaughey, J. O. O'Hara, and M. M. Thackeray, *Electrochem. Solid-State Lett.*, **3**, 13 (2000).
2. G. Herren and N. E. Walsoe de Reca, *Solid State Ionics*, **47**, 57 (1991).
3. R. A. Dunlap, D. E. Small, D. D. MacNeil, M. N. Obrovac, and J. R. Dahn, *J. Alloys Compd.*, **289**, 135 (1999).
4. W. A. Alexander, L. D. Calvert, R. H. Gamble, and K. Schinzel, *Can. J. Chem.*, **54**, 1052 (1976).
5. M. M. Thackeray, Paper 2 presented at the 10th International Meeting on Lithium Batteries, Como, Italy, May 28-June 2, 2000.
6. J. Wang, I. D. Raistrick, and R. A. Huggins, *J. Electrochem. Soc.*, **133**, 457 (1986).